Figure 4

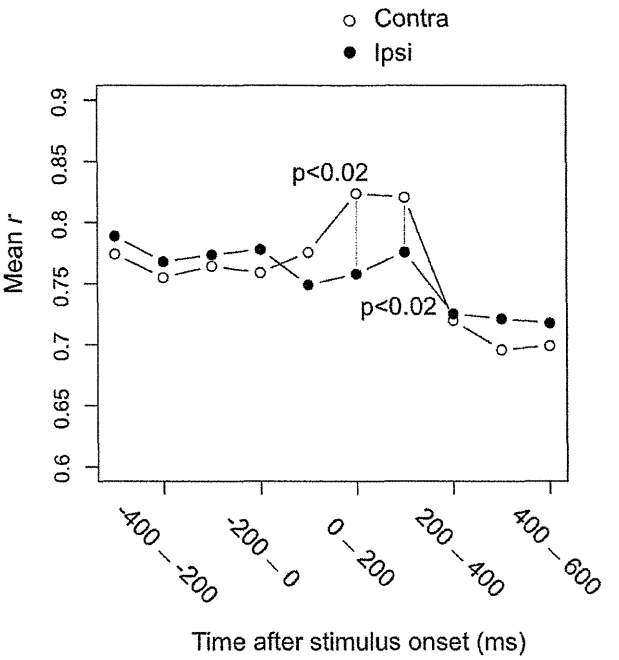
Contra
Ipsi
Mean r
0.6
0.65
0.7
0.75
0.8
0.85
0.9
p<0.02
p<0.02
-400 – -200
-200 – 0
0 – 200
200 – 400
400 – 600
Time after stimulus onset (ms)

Figure 5

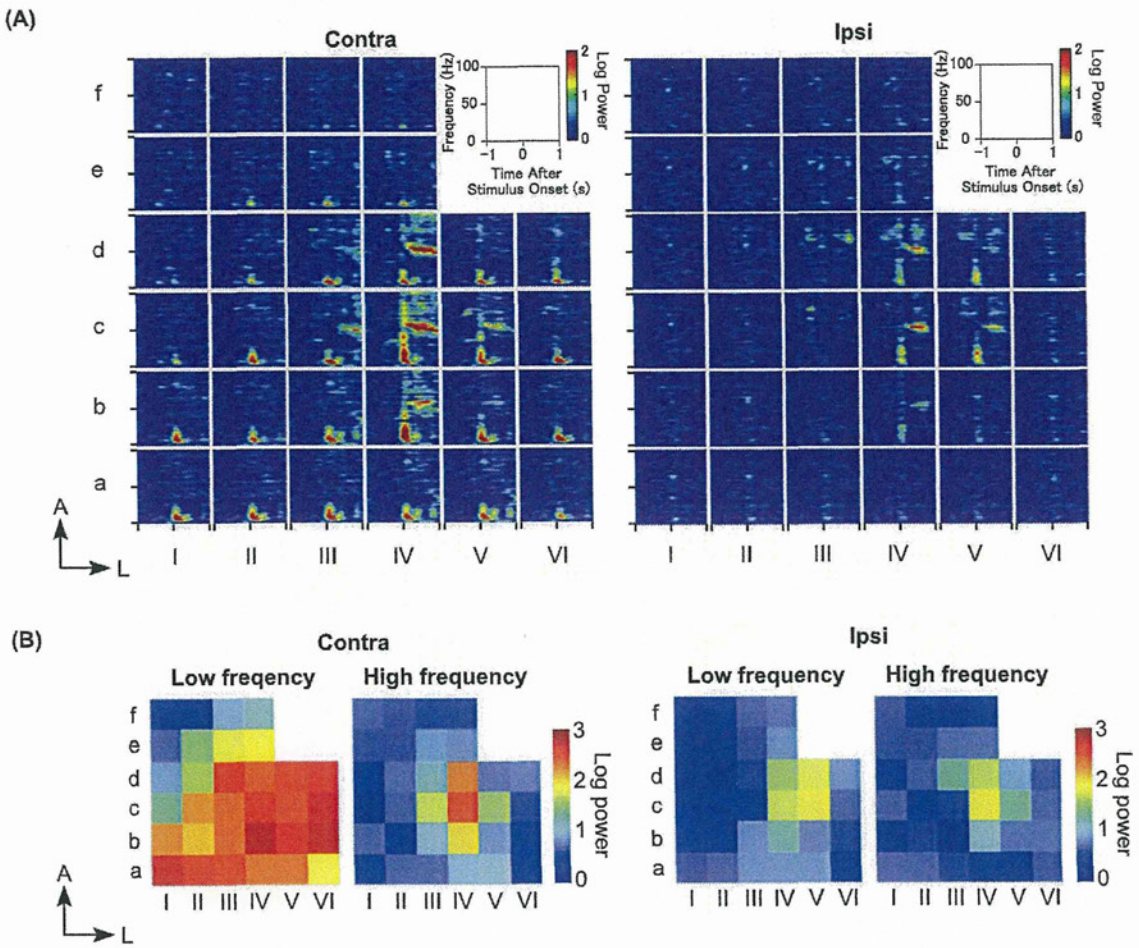
(A)
Contra
Ipsi
Frequency (Hz)
Log Power
Time After Stimulus Onset (s)
f
e
d
c
b
a
A
L
I II III IV V VI
(B)
Contra
Ipsi
Low freqency
High frequency
Low frequency
High frequency
Log power

Figure 6

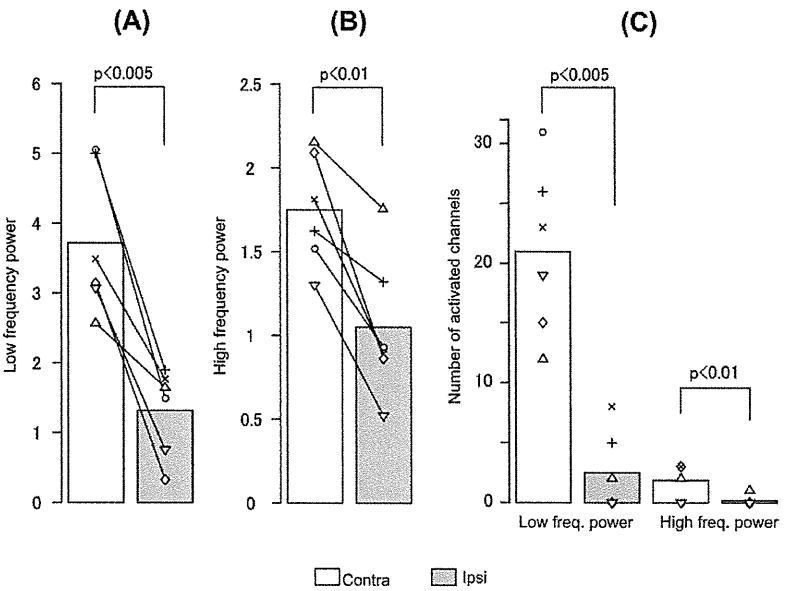
(A)
(B)
(C)
p<0.005
p<0.01
p<0.005
p<0.01
Low frequency power
High frequency power
Number of activated channels
Low freq. power
High freq. power
Contra
Ipsi

3D 映像視聴による自律神経系への影響

飯島淳彦　　小杉　剛　　木竜　徹　　長谷川功　　板東武彦

自律神経　第48巻　第3号　別刷
(2011年6月15日)

3D映像視聴による自律神経系への影響

飯島淳彦[a,b]　小杉　剛[b]　木竜　徹[b]　長谷川功[a]　板東武彦[a]

キーワード：映像酔い，立体酔い，瞳孔反応，動きベクトル，両眼視差
visually induced motion sickness, stereoscopic motion sickness, pupillary response, global motion vector, binocular disparity

はじめに

3D映像が急速に普及し，映画や家庭用テレビでも手軽に楽しめる時代がやってきた．これまで，2Dで視聴してきた映像が両眼視差を持つことにより，視聴者は迫力や臨場感，立体感と奥行き感を手に入れることになった．しかし手に汗握る興奮も度を越すと「映像酔い」「立体酔い」と呼ばれる映像による生体への悪影響が発現する．映像酔いは乗り物酔いの症状に似ており，映像の視聴によって吐き気，めまい感，頭痛，眼部不具合などが現れる．これらの酔い症状は主に自律神経系の反応だと言われている[1]．

本研究では，これまでに映像酔いを引き起こす可能性の高い映像の特徴抽出や，映像酔い症状の特徴やその発現メカニズムに関する研究を進めてきた．映像酔いをもたらす映像の多くは画面全体が大きく揺れるいわゆる「手ブレ映像」である．映像のブレは動きベクトル（グローバルモーションベクトル）として映像解析によって定量することができる[2]．動きベクトルは，パン（水平方向），ティルト（垂直方向），ロール（回転方向），ズーム（拡大縮小方向）の各成分に分離して分析でき，映像酔いと関係の深いベクトルの成分や大きさを探索してきた結果，3 Hz以下の緩やかな揺れを含む映像が映像酔いを引き起こしてきた可能性が示唆された[3]．また，立体映像に固有の問題としては，立体酔いが引き起こされることが指摘されている．視聴者に立体感を与える両眼視差が過度の場合に視聴者に不快感や眼精疲労がもたらされる[4]．立体酔いは映像に含まれる両眼視差に問題がある場合の他に，焦点調節と輻輳眼球運動の矛盾が主たる原因と考えられている[5]．

[a]新潟大学・医歯学系・統合生理学分野
〒951-8510　新潟県新潟市中央区旭町通1—757
[b]新潟大学・自然科学系・人間支援科学分野
〒950-2181　新潟県新潟市西区五十嵐2の町8050

1. 映像視聴実験

これらの症状を的確に把握するため，映像視聴中の被験者の瞳孔反応・眼球運動，心電図，連続血圧や呼吸などを同時計測し，映像と生理学的指標との関係を調べてきた（図1）．眼球運動の解析では，被験者の視線と刺激映像との関係や映像に含まれる物理量がどのように眼球運動の発現に寄与するか検証してきた．3D映像からは両眼視差を求め，被験者の視線データに基づき実際に被験者が見ている両眼視差を定量し，その量と輻輳開散眼球運動（vergence）の大きさを比較した．その結果，3D映像の視聴においてその視差量に応じたvergenceが観察されるのはもちろんのこと，3D映像から視差を除去した2D映像においてもvergenceの観察されたシーンがあった[3]．これは，立体感をもたらす両眼視差以外のキュー（例えば，物体の陰影や大小関係，大きさの変化など）によって誘発されたvergenceと考えられる．またoptic flowも持続的なvergenceに貢献することが分かった[3]．

映像視聴実験において，映像酔いを議論する上で重要なのが自律神経系の変化である．本研究では，瞳孔反応，心電図，連続血圧，呼吸数の計測から自律神経系指標を抽出して分析を進めている．なお，映像酔いの度合いを判定する心理的指標としては，シミュレータ酔いの指標として古くから用いられてきているSSQ（Simulator Sickness Questioner）[6]と呼ばれるアン

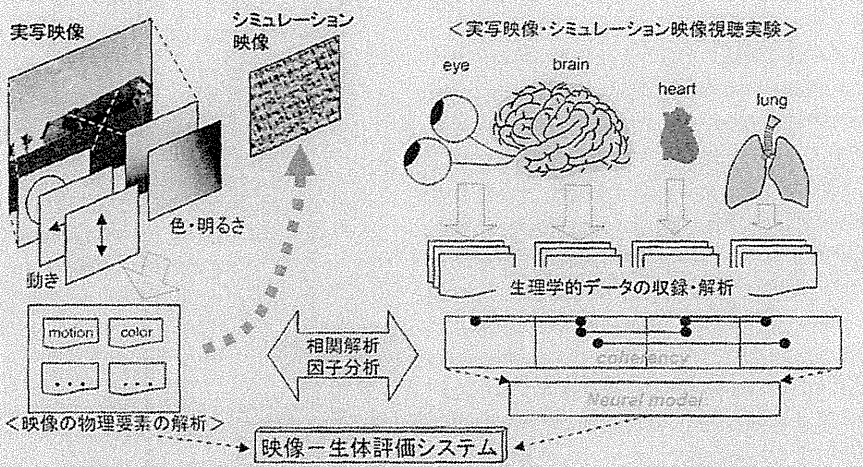

図1 映像視聴実験の全体像
映像に含まれる物理量の解析（動きベクトル，両眼視差，色や明るさの時系列情報）と被験者から得られる生理学的指標との関連を精査する．

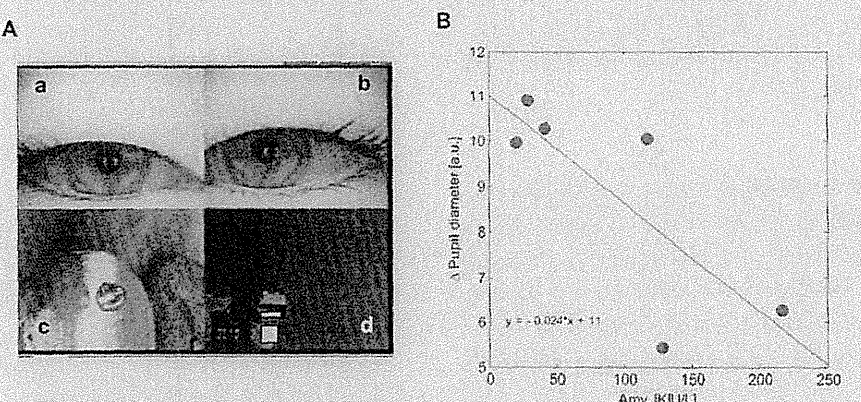

図2 映像視聴実験における瞳孔変化量と唾液アミラーゼの関係
A：視聴中の被験者の眼球（a，b）と被験者の見ている刺激画面（c），および被験者の視聴している様子（d）．
B：唾液中アミラーゼ量（横軸）に対する瞳孔変化量（縦軸），両者の関係には負の相関が見られた．

ケート法を用いた．この中で，「Nausea」，「Oculomoter」，「Disorientation」の3項目のスコアを用いて酔いの有無の判定を行った[9]．心電図から得られる心拍波形のRR間隔の揺らぎ，血圧変動，呼吸変化の周波数解析より，映像によって酔い症状が現れた被験者では交感神経系の活動が大きくなる傾向を確認した[9]．これは自律神経系に見られる映像酔いの特徴だと考えられる．

2. 映像視聴と瞳孔反応

瞳孔は交感神経と副交感神経の2重支配を受けており，散瞳と縮瞳のバランスを観察することで自律神経系の状態を推定することが可能である．本研究では，循環系の指標と同時に，瞳孔反応を用いて映像視聴に伴う自律神経系の変化を評価した．3D映像による生体影響を映像視聴前後の対光反射量で検討した実験で

は，被験者が主張する映像の不快感と対光反射量が相関した[8]．

そもそも映像は画面の明るさ変化に富む刺激であることから，映像そのものを光刺激として瞳孔反応を調べることが可能である．そこで映像の輝度変化と瞳孔反応に注目した実験を行った．被験者は10秒毎に合計18種類の映像が呈示される刺激を注視し，その際の瞳孔反応を解析した．映像視聴中の瞳孔反応は，被験者の視界を妨げることなく眼球運動・瞳孔反応を記録できるゴーグル型眼球解析システム（ET-60u，ニューオプト社）を用いて解析した．今回は180秒間の映像呈示期間中の最大瞳孔径と最小瞳孔径の差を瞳孔変化量として注目し，更に瞳孔と別の自律神経系生理指標との関係を明らかにするため，唾液中アミラーゼをもう一つの指標とした．唾液中アミラーゼはストレス状態の推定に有効とされ，口腔内で検査紙を唾液に浸し唾液アミラーゼモニタ（ニプロ社）で定量した．図2には映像視聴実験中の瞳孔反応量と唾液中アミラーゼとの関係を示した．アミラーゼ高値の被験者ほど瞳孔反応量が小さいという結果が得られた．これによれば，強いストレス状態で自律神経系が正常に機能していないことが予測される．

まとめ

3D映像を含む映像全般が生体に与える影響について，自律神経系のパラメータに注目して解析した．瞳孔，循環系のパラメータを組み合わせてみることで，より詳細に自律神経の機能を評価することが可能である．本法は映像に対する生体反応全般の解析から，映像そのものの評価に至るまで幅広い活用が期待される．

謝辞：本研究の一部は，(財) 塚田医学奨学基金，(財) エヌ・エス知覚科学振興財団，(財)中山科学振興財団，新潟大学プロジェクト推進経費の各助成を受けて実施した研究の成果である．また，(財) JKAの機械工業振興事業補助金の交付を受けて行った（財）機械システム振興協会の平成21年度委託事業「映像刺激を用いた心理的負荷測定システムの開発に関するフィージビリティスタディ」として実施したものの一部も含まれる．関係各位に御礼申し上げる．

文　献

1) Cowings PS, Suter S, Toscano WB, et al. General autonomic components of motion sickness. Psychophysiology 1986; 23: 542—551.
2) 映像酔いガイドライン検証システムの実用化に関するフィージビリティスタディ報告書．財団法人機械システム振興協会；2008.
3) Iijima A, Kiryu T, Ukai K, et al. Vergence eye movements elicited by non-disparity factors in 2D realistic movies. In: The First International Symposium on Visually Induced Motion Sickness, Fatigue, and Photosensitive Epileptic Seizures (VIMS 2007). 2007. p. 59—66.
4) 秦泉寺久美，石橋　聡，小林直樹．カメラモーション抽出による多層スプライト自動生成．電子情報通信学会和文論文誌（D-II）1999；J82-D-II：1018—1030.
5) Kennedy RS, Lane NE, Berbaum KS, et al. A simulator sickness questionnaire: An enhanced method for quantifying simulator sickness. The International Journal of Aviation Psychology 1993; 3: 203—220.
6) 小杉　剛，飯島淳彦，木竜　徹．高臨場感映像のダイナミクスが心拍変動に与える影響の評価法に関する検討．第25回生体生理工学シンポジウム論文集．2010. p. 103—104.
7) Okada Y, Ukai K, Wolffsohn JS, et al. Target spatial frequency determines the response to conflicting defocus- and convergence-driven accommodative stimuli. Vision Res 2006; 46: 475—484.
8) Oyamada H, Iijima A, Tanaka A, et al. A pilot study on pupillary and cardiovascular changes induced by stereoscopic video movies. J Neuroeng Rehabil 2007; 4: 37.
9) 蘇日塔拉図，外山　寛，小杉　剛ら．事前運動と映像注視が映像酔いおよび心拍に与える影響．生体医工学　2010；48：98—105.
10) Ukai K, Howarth P. Visual fatigue caused by viewing stereoscopic motion images: Background, theories, and observations. Displays 2008; 29: 106—116.

Neuroscience 193 (2011) 249–258

LOCAL AND RETROGRADE GENE TRANSFER INTO PRIMATE NEURONAL PATHWAYS VIA ADENO-ASSOCIATED VIRUS SEROTYPE 8 AND 9

Y. MASAMIZU,[a1] T. OKADA,[b] K. KAWASAKI,[c] H. ISHIBASHI,[a] S. YUASA,[d] S. TAKEDA,[b] I. HASEGAWA[c] AND K. NAKAHARA[a]*

[a]*Department of Neurophysiology, National Institute of Neuroscience, NCNP, 4-1-1 Ogawa-Higashi, Kodaira, Tokyo 187–8502, Japan*

[b]*Department of Molecular Therapy, National Institute of Neuroscience, NCNP, 4-1-1 Ogawa-Higashi, Kodaira, Tokyo 187–8502, Japan*

[c]*Department of Physiology, Niigata University School of Medicine, 1 Asahimachi-dori, Niigata, Niigata 951-8510, Japan*

[d]*Department of Ultrastructural Research, National Institute of Neuroscience, NCNP, 4-1-1 Ogawa-Higashi, Kodaira, Tokyo 187–8502, Japan*

Abstract—Viral vector-mediated gene transfer has become increasingly valuable for primate brain research, in particular for application of genetic methods (e.g. optogenetics) to study neuronal circuit functions. Neuronal cell tropisms and infection patterns are viable options for obtaining viral vector-mediated transgene delivery that is selective for particular neuronal pathways. For example, several types of viral vectors can infect axon terminals (retrograde infections), which enables targeted transgene delivery to neurons that directly project to a particular viral injection region. Although recent studies in rodents have demonstrated that adeno-associated virus serotype 8 (AAV8) and 9 (AAV9) efficiently transduce neurons, the tropisms and infection patterns remain poorly understood in primate brains. Here, we constructed recombinant AAV8 or AAV9, which expressed an enhanced green fluorescent protein (EGFP) gene driven by a ubiquitous promoter (AAV8-EGFP and AAV9-EGFP, respectively), and stereotaxically injected it into several brain regions in marmosets and macaque monkeys. Immunohistochemical analyses revealed almost exclusive colocalization of EGFP fluorescence via AAV9-mediated gene transfer with a neuron-specific marker, indicating endogenous neuronal tropism of AAV9, which was consistent with our previous results utilizing AAV8. Injections of either AAV8-EGFP or AAV9-EGFP into the marmoset striatum resulted in EGFP expression in local striatal neurons as a result of local infection, as well as expression in dopaminergic neurons of the substantia nigra via retrograde transport along nigrostriatal axonal projections. Retrograde infections were also observed in the frontal cortex and thalamus, which are known to have direct projections to the striatum. These local and retrograde gene transfers were further demonstrated in the geniculocortical pathway of the marmoset visual system. These findings indicate promising capabilities of AAV8 and AAV9 to deliver molecular tools into a range of primate neural systems in pathway-specific manners through their neuronal tropisms and infection patterns.

Key words: AAV8, AAV9, common marmoset, gene transfer, macaque monkey, neuronal pathway.

The utilization of nonhuman primates as animal models for neuroscience research has provided a better understanding of mechanisms of high-level brain functions (Felleman and Van Essen, 1991; Nakahara et al., 2007; Passingham, 2009). Although lesion, anatomical and electrophysiological studies have revealed neural substrates and activities in primate brains, the lack of effective methods has hampered efforts to correlate detailed neural circuits with functions. Recently developed genetic methods provide promise for facilitating such studies, especially by the use of genetically encoded modulators, which have the ability to turn neuronal activity on or off with high spatiotemporal precision (Tan et al., 2006; Zhang et al., 2007; Han et al., 2009). A major hurdle for the application of genetic methods has been the specific *in vivo* expression of transgenes encoding relevant molecules in neurons of the central nervous system (CNS). In primates, although a few cases have proven successful (Chan et al., 2001; Sasaki et al., 2009), the use of generations of transgenic animals remains impractical. Therefore, gene transfer vectors could serve as a useful method for delivering transgenes into the primate CNS.

Adeno-associated viruses (AAV) are used as transgene vectors within the CNS, because they can readily infect postmitotic cells (Kaplitt et al., 1994; Kaspar et al., 2002; Hollis et al., 2008; Towne et al., 2010). Diverse AAV serotypes exist because of variations of capsid proteins, which also act as tropism determinants. Although the AAV serotype 2 (AAV2) has been most frequently used, recent attempts have sought to determine suitable AAV serotypes for target cell types, tissues, and species (Gao et al., 2002, 2004; Tan et al., 2006). Rodent studies have demonstrated that AAV8 and AAV9 are suitable for transgene deliveries into neuronal cells (Broekman et al., 2006; Taymans et al., 2007; Foust et al., 2009, 2010), and recently, we and

[1] Present address: Division of Brain Circuits, National Institute for Basic Biology, Nishigonaka 38, Myodaiji, Okazaki, Aichi 444-8585, Japan.

*Corresponding author. Tel: +81-42-346-1724; fax: +81-42-346-1754.
E-mail address: nakahara@ncnp.go.jp (K. Nakahara).

Abbreviations: AAV8, adeno-associated virus serotype 8; AAV9, adeno-associated virus serotype 9; CAG, modified chicken β-actin promoter with a cytomegalovirus immediate early enhancer; CNS, central nervous system; DA, dopamine; EGFP, enhanced green fluorescent protein; GFAP, glial fibrillary acidic protein; LGN, lateral geniculate nucleus; NeuN, neuron-specific nuclear protein; Olig2, oligodendrocyte transcription factor 2; PBS, phosphate-buffered saline; PCR, polymerase chain reaction; SNc, substantia nigra pars compacta; SNr, substantia nigra pars reticulata; TH, tyrosine hydroxylase; WPRE, woodchuck hepatitis virus post-transcriptional regulatory element.

0306-4522/11 $ - see front matter © 2011 IBRO. Published by Elsevier Ltd. All rights reserved.
doi:10.1016/j.neuroscience.2011.06.080

others showed that AAV8 exhibits strong tropism for neurons in marmoset (Masamizu et al., 2010) and macaque monkey (Dodiya et al., 2010) brains. However, AAV9, another promising neurotropic serotype, has not yet been tested on primate brains.

Several AAV serotypes can transfer genes into neurons via local and retrograde infection. Although local infections from neuronal somata and/or dendrites allow for gene transfer into neurons surrounding the virus administration sites, retrograde infections from axon terminals provide axonal transport of viral genomes. This results in transgene expression in neuronal somata of distal regions that project to the virus administration sites, which could provide strategies for transgene delivery targeted to specific neuronal pathways. For instance, AAV-mediated retrograde gene transfers have been successful in the substantia nigra and in spinal cord motoneurons (Yasuda et al., 2007; Towne et al., 2010). Exploring the infection patterns of AAV8 and AAV9 in primate brains is, therefore, a prerequisite for utilizing these serotypes in a neuronal pathway-specific manner.

The present study initially analyzed the cell tropism of AAV9 in common marmoset and macaque monkey brains. Subsequently, we explored the infection patterns of either AAV8 or AAV9 in the marmoset brain after injection into the striatum to determine the ability of retrograde infection. Moreover, the utilization of this gene transfer strategy was demonstrated by successful application of AAV8 and AAV9 to the geniculocortical pathway of the visual system.

EXPERIMENTAL PROCEDURES

Animals

Five adult, male, common marmosets (*Callithrix jacchus*) and two adult, male, macaque monkeys (*Macaca mulatta* and *Macaca fuscata*) were used for the present study (Table 1). The marmosets were 20–59 months old (230–325 g), and the macaques were 8 years old (9.2 kg) and 7 years old (6.2 kg) at the start of the experiment. All experiments were conducted in accordance with protocols approved by the ethics committee for primate research at the National Center of Neurology and Psychiatry, Japan.

Virus production

Recombinant AAV8 and AAV9 expressing enhanced green fluorescent protein (EGFP) were produced (AAV8-EGFP and AAV9-EGFP, respectively) as previously described (Okada et al., 2005, 2009). The vector plasmid (pAAV-EGFP) contained EGFP cDNA and the woodchuck hepatitis virus post-transcriptional regulatory element (WPRE), which was expressed under control of the CAG promoter, a modified chicken β-actin promoter with a cytomegalovirus immediate early enhancer. AAV8-EGFP and AAV9-EGFP viruses were produced following triple-transfection of HEK293 cells with pAAV-EGFP, an adenoviral helper plasmid pAdeno (Matsushita et al., 1998), and a chimeric helper plasmid encoding either AAV2 rep/AAV8 cap genes or AAV2 rep/AAV9 cap genes (pAAV2-8, pAAV2-9, respectively, gifts from Dr. James M. Wilson) (Gao et al., 2002, 2004), which was mediated by calcium phosphate co-precipitation with active gassing (Okada et al., 2005). At 72 h after transfection, cell suspensions were collected, centrifuged at 300×*g* for 10 min, and resuspended in 30 ml Tris-buffered saline (100 mM Tris–HCl [pH 8.0], 150 mM NaCl). AAV8-EGFP and AAV9-EGFP viruses were harvested by five-cycle freeze-thawing of the resuspended pellet. The crude viral lysate was initially concentrated by a brief two-tier CsCl gradient centrifugation for 3 h (Okada et al., 2002) and further purified by dual ion-exchange chromatography (Okada et al., 2009). Quantitative polymerase chain reaction of DNase I-treated stocks with plasmid standards determined the final number of AAV8-EGFP and AAV9-EGFP virus particles as 3.0×10^{13} and 9.27×10^{12} vector genomes (vg)/ml, respectively.

Table 1. Injection sites and viral vectors in marmosets and macaques

	Striatum		Primary visual cortex	
Animal	Right	Left	Right	Left
Marmoset A		AAV9		
Marmoset B		AAV9		
Marmoset C		AAV8		
Marmoset D			AAV9	
Marmoset E			AAV9	AAV8
Macaque A				AAV9
Macaque B			AAV8	AAV9

Virus injection

All surgical procedures and virus injections were conducted under aseptic conditions. Animals were initially i.m. anesthetized with 15–22 mg/kg of ketamine (for marmosets) or with 5 mg/kg of ketamine and 0.03 mg/kg of medetomidine (for macaques), followed by intubation and placement in a stereotaxic apparatus. Anesthesia was then maintained with inhalation of isoflurane (1.5–2.5% in oxygen). Saturation of pulse oxygen (SpO_2), heart rate, body temperature, end-tidal CO_2 ($ETCO_2$) and O_2 (ETO_2), isoflurane (ETISO), and fraction of inspired CO_2 ($FiCO_2$), O_2 (FiO_2), and isoflurane (FiISO) were continuously monitored. Following i.m. injection of the antibiotic cefovecin, a small craniotomy (2–3 mm in diameter) was made over the area of interest, and the underlying dura was slit to allow penetration of the virus-containing 10-μl Hamilton syringe connected to a 33 G (45° angle) needle. The viral solution (3 μl) was injected at a rate of 0.25 μl/min at each site. Injection sites were determined with a stereotaxic atlas of the marmoset brain (Yuasa et al., 2010) and the macaque brain (BrainMaps.org, http://brainmaps.org/), respectively. The marmoset injection sites were aimed at the striatum: 12.0 mm anterior from the interaural line, 3.0 mm lateral (L) from the midline and 6.0 mm ventral (V) from the brain surface (Eslamboli et al., 2005), as well as the primary visual cortex: 10.0 mm posterior from the interaural line, 5.0 mm L, and 2.5 mm V (Fritsches and Rosa, 1996). After each injection, the needle was maintained in place for an additional 5 min (striatum) or 15 min (primary visual cortex), and then slowly withdrawn (2 mm/min). The macaque injection sites were aimed at the primary visual cortex. After each injection, the needle was maintained in place for an additional 5 min, and then slowly withdrawn (2 mm/min).

Immunohistochemistry

Procedures were performed as previously described (Nakahira and Yuasa, 2005; Masamizu et al., 2010). At 4 weeks postinjection, animals were deeply anesthetized with a sodium pentobarbital overdose and transcardially perfused with 4% paraformaldehyde in 0.1 M phosphate-buffered saline (PBS, pH 7.4). Brains were removed from the skull and postfixed at 4 °C for 2–3 days using the same fresh fixative. The brains were embedded in 3% agar/PBS and sliced into 100-μm thick coronal sections using a Microslicer (DTK-3000, Dosaka EM, Kyoto, Japan). After 1 h of preincubation with 10% normal goat serum at 4 °C, floating sec-

tions were incubated with primary antibodies in PBS/2% Triton X-100 at 4 °C overnight. Antibodies against the following neuronal or glial marker proteins were used: neuron-specific nuclear protein (NeuN; mouse IgG, 1:500; Cat. No. MAB377, Millipore, Billerica, MA, USA), tyrosine hydroxylase (TH; mouse IgG, 1:1000; Cat. No. T2928, Sigma-Aldrich, St. Louis, MO, USA), glial fibrillary acidic protein (GFAP; rabbit IgG, 1:200; Cat. No. Z0334, Dako, Glostrup, Denmark), and oligodendrocyte transcription factor 2 (Olig2; rabbit IgG, 1:2000 Cat. No. AB9610, Millipore, Billerica, MA, USA). Following PBS rinses, the sections were incubated with secondary antibodies in PBS at 4 °C for 5 h. Secondary antibodies (Alexa goat anti-mouse 594 IgG [1:500; Cat. No. A11005, Molecular Probes, Eugene, OR, USA] or Alexa goat anti-rabbit 594 IgG [1:500; Cat. No. A11012, Molecular Probes, Eugene, OR, USA]), which were directed against the species in which the primary antibody was raised, were used in each case.

Imaging, cell quantification, and statistics

Brain sections were mounted on glass slides with Fluoromount-G (Beckman Coulter, Fullerton, CA, USA). Immunofluorescence and EGFP fluorescence were observed under a confocal laser-scanning microscope (LSM5 Pascal, Zeiss, Oberkochen, Germany) at a resolution of 1024×1024 pixels and one confocal plane. Co-expression of NeuN, GFAP, or Olig2 with EGFP-fluorescence was quantified using ImageJ software (National Institute of Health, Bethesda, MD, USA, http://rsb.info.nih.gov/ij/) with a 40× objective lens. For cell counting analyses, we examined 5–12 microscopic fields in two to four adjacent sections in each case. The number of EGFP-positive cells was statistically analyzed by the chi-square test using JMP8 (SAS Institute, Cary, NC, USA).

Viral transgene detection

Brain slices prepared as in the immunohistochemical analyses (see above) were used for the viral transgene detection assay. Small volumes of tissue were sampled from the injection sites and from regions that contained neuron populations expressing retrograde EGFP labels, under the guidance of EGFP fluorescence by microscopic observation. Extraction and polymerase chain reaction (PCR) amplification of total DNA were performed using the KAPA MG Kit (Cat. No. KK7153, Kapa Biosystems, Woburn, MA, USA). Viral transgenes were detected by PCR using the EGFP (5′-TATATCATGGCCGACAAGCA-3′) and WPRE (5′-CCACATAGCGTAAAAGGAGCA-3′) primers. For internal controls, β-actin DNA was amplified using the primers for β-actin 001 (5′-TCCTGACCCTGAAGTACCCC-3′) and β-actin 002 (5′-GTGGTGGTGAAGCTGTAGCC-3′) (Sasaki et al., 2009).

Thirty-five cycles of PCR were performed (15 s each at 95, 62, and 72 °C) in between an initial denaturation at 95 °C for 3 min and a final elongation at 72 °C for 10 min. PCR products were analyzed by electrophoresis on a 1.2% agarose gel.

RESULTS

Preferential neuronal tropism of AAV9 in marmoset and macaque brains

We have previously shown that AAV8 exhibits a strong tropism for neurons, but not for glia, in the marmoset brain (Masamizu et al., 2010). The present study aimed to determine the tropism of AAV9, which is another promising neurotropic serotype, in the marmoset brain. Recombinant AAV9 expressing the EGFP gene under the CAG promoter (AAV9-EGFP) was generated and stereotaxically injected into the striatum of two marmoset monkeys (Fig. 1A). Four weeks after injection, striatal sections were observed with a confocal microscope. EGFP fluorescence was visible in numerous cell bodies and processes around the injection site (Fig. 1B). Immunohistochemistry revealed that almost all EGFP-positive cells also expressed NeuN (Fig. 1D). Computer-aided cell counting revealed that 99% of EGFP-positive cells also expressed NeuN (Table 2). In contrast, co-expression of EGFP-positive cells with the astrocyte marker GFAP or the oligodendrocyte marker Olig2 was rarely detected (Fig. 1E, F, Table 2). Frequencies of co-localization of cell type-specific markers with EGFP signals were significantly different across cell types ($P<0.0001$, chi-square test; Table 2). Because CAG promoter activity was expected to be ubiquitous across neuronal and glial cell types, these results indicate strong endogenous neuronal tropism of AAV9.

AAV9 neurotropism was also observed in the macaque monkey, the most widely used primate model animal in neuroscience research. AAV9-EGFP was injected into the primary visual cortex of two macaque monkeys. EGFP fluorescence was coexpressed almost exclusively with NeuN, but rarely with glial markers (Fig. 2).

Viral gene transfers to neuronal pathways after the striatum infection

To date, AAV8 and AAV9 infection patterns (local infection from cell bodies/dendrites or retrograde infection from axon terminals) in primate brains have not been elucidated; however, the reciprocal projections between the striatum and substantia nigra offer an appropriate model system for analyzing this. GABAergic neurons in the striatum project to the substantia nigra pars reticulata (SNr), and dopaminergic neurons in the substantia nigra pars compacta (SNc) project to the striatum (Albin et al., 1989; Alexander and Crutcher, 1990; Minamimoto et al., 2009) (Fig. 3B). Therefore, either AAV8-EGFP or AAV9-EGFP was injected into the marmoset striatum, followed by analysis of EGFP expression in the SNr and SNc, ipsilateral to the injection side (Fig. 3A). For both vectors, strong EGFP fluorescence was directly observed in axon terminals in the SNr, as well as in cell bodies of the SNc (Fig. 3C, F). Almost all EGFP-positive cells in the SNc were dopaminergic neurons, as revealed by co-expression of TH (Fig. 3D, G), indicating retrograde EGFP gene transfers after the viral infection in the striatum. We counted the number of EGFP-positive cells among TH-positive neurons to estimate efficacy of retrograde gene transfers. Proportions of EGFP-positive cells among TH-positive neurons were 38% for AAV8 (EGFP-positive/TH-positive: 81/216), and 49% for AAV9 (EGFP-positive/TH-positive: 102/208). In the SNr, high-power confocal images revealed EGFP-positive fibers and varicosities surrounding NeuN-positive cell bodies (Fig. 3E, H). These results suggested that an AAV8-EGFP or AAV9-EGFP injection into the striatum resulted in anterograde transport of transgene products to nerve terminals in the SNr via the striatonigral pathway, as well as retrograde transport of the transgene to cell bodies in the SNc via the nigrostriatal dopaminergic pathway (Fig. 3B).

The striatum receives major projections from the thalamus and the cerebral cortex (Alexander and Crutcher,

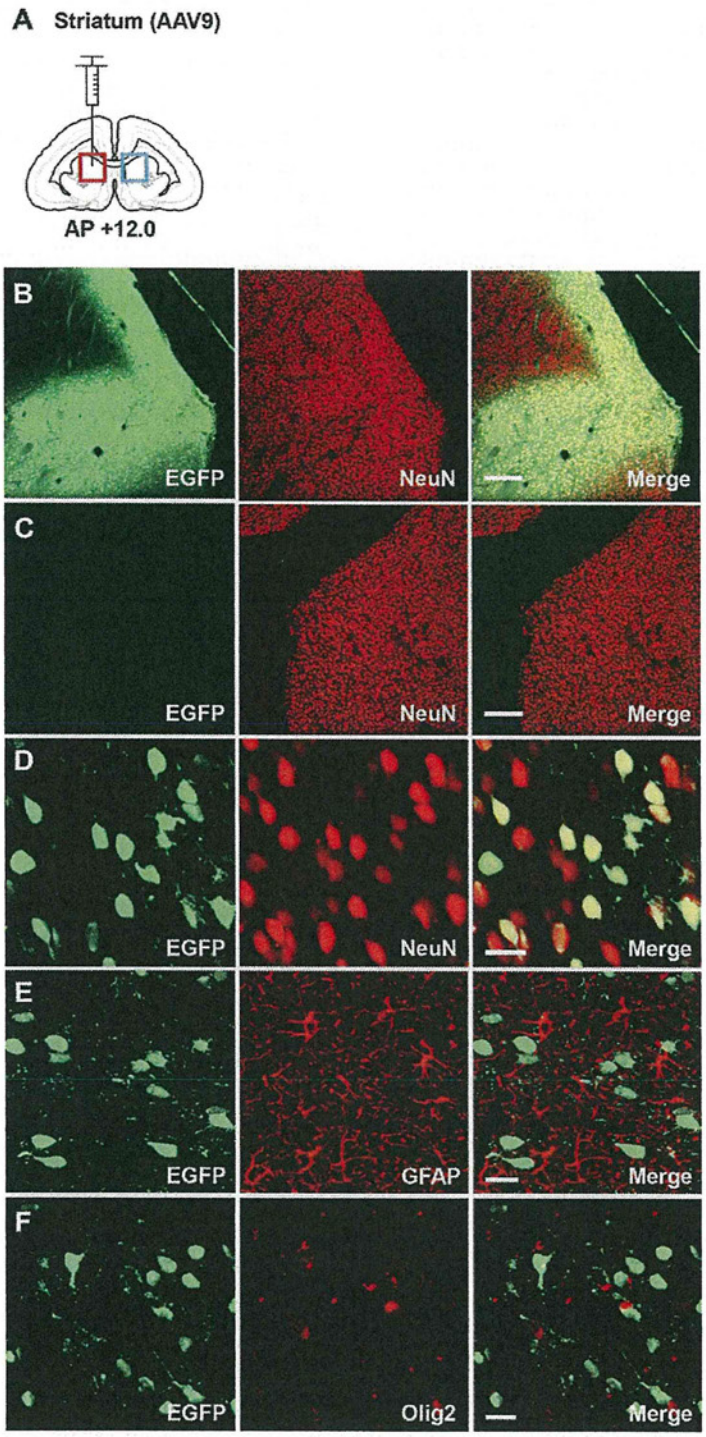

Fig. 1. Efficient gene transfer into neurons of the marmoset striatum using AAV9. (A) The striatal injection site is indicated on a coronal section of the marmoset brain, approximately 12 mm anterior to the interaural line. (B) Low power confocal images corresponding to the red box on the coronal marmoset brain map in (A). Native EGFP fluorescence (left, green), NeuN immunofluorescence signal (center, red), and the merged image (right) are shown. (C) Images of the noninjected control side corresponding to the light-blue box in (A). (D) Confocal images of high-power fields reveal that EGFP-positive cells (green) co-express NeuN (red), as shown by the merged image (yellow). (E, F) EGFP-positive cells (green) rarely co-express GFAP (E; red) or Olig2 (F; red). Bars=200 μm in (B, C) and 20 μm in (D–F). AAV9, adeno-associated virus serotype 9; AP, anteroposterior; EGFP, enhanced green fluorescent protein; GFAP, glial fibrillary acidic protein; NeuN, neuron-specific nuclear protein; Olig2, oligodendrocyte transcription factor 2.

Table 2. Proportion of cells expressing NeuN, GFAP, or Olig2 in EGFP-positive cells in the striatum and primary visual cortex of marmosets following AAV8-EGFP or AAV9-EGFP viral injection

Injection site	Neuron ($NeuN^+/EGFP^+$ cells)	Astrocyte ($GFAP^+/EGFP^+$ cells)	Oligodendrocyte ($Olig2^+/EGFP^+$ cells)
Striatum (AAV8)	98% (484/494)	0% (0/497)	1% (5/500)
Striatum (AAV9)	99% (492/495)	0% (0/500)	1% (3/497)
Primary visual cortex (AAV8)	99% (490/497)	0% (0/502)	1% (3/498)
Primary visual cortex (AAV9)	98% (494/505)	0% (0/493)	1% (5/502)

In all cases, the frequencies of colocalization of cell type-specific markers with EGFP signals are significantly different across cell types ($P<0.0001$, chi-square-test).

1990; Minamimoto et al., 2009). Thus, we also sought retrogradely infected neurons in these regions. We found EGFP expressing neuronal somata in the thalamus probably corresponding to the parafascicular thalamic nucleus (Fig. 4B) (Minamimoto et al., 2009; Yuasa et al., 2010). Neurons expressing EGFP were also found in the frontal and insular cortices at almost the same anterior–posterior level as the striatal injection site (Fig. 4C, D) (Yuasa et al., 2010).

To further confirm retrograde neuronal infections by AAV8 and AAV9, we aimed to detect AAV transgenes in neurons with retrograde EGFP labels. We extracted total DNA from small areas of the frontal/insular cortices and the thalamus where retrograde EGFP labels were observed, and performed PCR using the primers complimentary to a sequence within the AAV construct. For both AAV8 and AAV9, we detected the presence of viral transgenes in the frontal/insular cortices and in the thalamus (Fig. 4E), indicating the viral transgene itself was transported to remote somata after retrograde infections with AAV8 or AAV9.

Local and retrograde gene transfer to the geniculocortical pathway

Gene transfer capabilities of AAV8 and AAV9 were subsequently analyzed in the marmoset visual system. The primary visual cortex (V1) and lateral geniculate nucleus (LGN) constitute reciprocal loops typical for corticothalamic pathways: feedforward projections from the LGN to V1 and feedback projections from the V1 to LGN (Felleman and Van Essen, 1991; Murphy and Sillito, 1996). Either AAV8-EGFP or AAV9-EGFP were injected into the marmoset V1, aiming at the region representing foveal retinotopy, according to previously described electrophysiological mappings (Fritsches and Rosa, 1996). Following injection, EGFP signals were observed across cortical layers at the injection site, and AAV8 and AAV9 neuronal tropisms were confirmed by nearly complete co-expression with NeuN (Table 2). EGFP fluorescence was then detected in the ipsilateral LGN (Fig. 5 for AAV9-EGFP; data not shown for AAV8-EGFP), demonstrating that V1 injection of either AAV8-EGFP or AAV9-EGFP resulted in EGFP expression in the LGN, which was in apparent retinotopic correspondence with the V1 injection site (White et al., 1998) (Fig. 5B). The EGFP labels were apparently restricted to the parvocellular layer (White et al., 1998). In confocal images with high-power magnification, EGFP-positive axons and varicosities were clearly identified (Fig. 5D), suggesting anterograde transport of the transgene products (EGFP) via projections from the V1 to LGN. Neuronal somata also expressed EGFP in the LGN, suggesting retrograde axonal transport of the transgene from the V1 injection site (Fig. 5D). Efficacy of retrograde infections in the LGN were relatively low compared with that in the SNc. Proportions of EGFP-positive cells among NeuN-positive neurons were 15% for AAV8 (EGFP-positive/NeuN-positive: 26/170) and 22% for AAV9 (EGFP-positive/NeuN-positive: 38/173).

DISCUSSION

The present study demonstrated that AAV9 efficiently and selectively infected neurons *in vivo* in the marmoset brain (Fig. 1). This neuronal tropism was similar to that of AAV8, which was shown in our previous study (Masamizu et al., 2010). Results from the present study, in combination with our preliminary results, demonstrate strong AAV8 and AAV9 neurotropism in the brains of macaque monkeys, the most widely used primate animal model in neuroscience research (Fig. 2 for AAV9, data not shown for AAV8). These results suggest that AAV8 and AAV9 exhibit a wide range of neuronal infection across primate species, possibly including humans. To obtain selective transgene expression in neurons, neuron-specific promoters, such as the CaMKII promoter, are used typically. However, neuron-specific promoter activity is often weak and insufficient for effective transgene expression. Endogenous AAV8 and AAV9 tropisms permit efficient and almost exclusive neuronal transgene expression through the use of ubiquitous, strong promoters, such as the CAG promoter, rather than specific, weak promoters.

Recently, Foust et al. (2009, 2010) reported that intravascular injection of AAV9 allows transduction of neurons throughout the brain in newborn mice, as well as in spinal motoneurons of newborn cynomolgus monkeys. In adult mice, however, i.v. delivery of AAV9 results in preferential transduction of astrocytes, rather than neurons. In the present study, AAV9 infected, almost exclusively, neurons in the adult marmoset and macaque brain via direct virus injection into the parenchyma. The discrepancy in cell tropism may be attributed to species differences and/or differences in brain entry: i.v. vs. parenchyma injection. The structure of genomes and the purification procedure of viral particles may also affect cell tropism of AAV vectors. Here, we used conventional single-stranded AAV9 purified with ion-exchange chromatography, whereas Foust et al. used double-stranded, self-complementary AAV9 purified

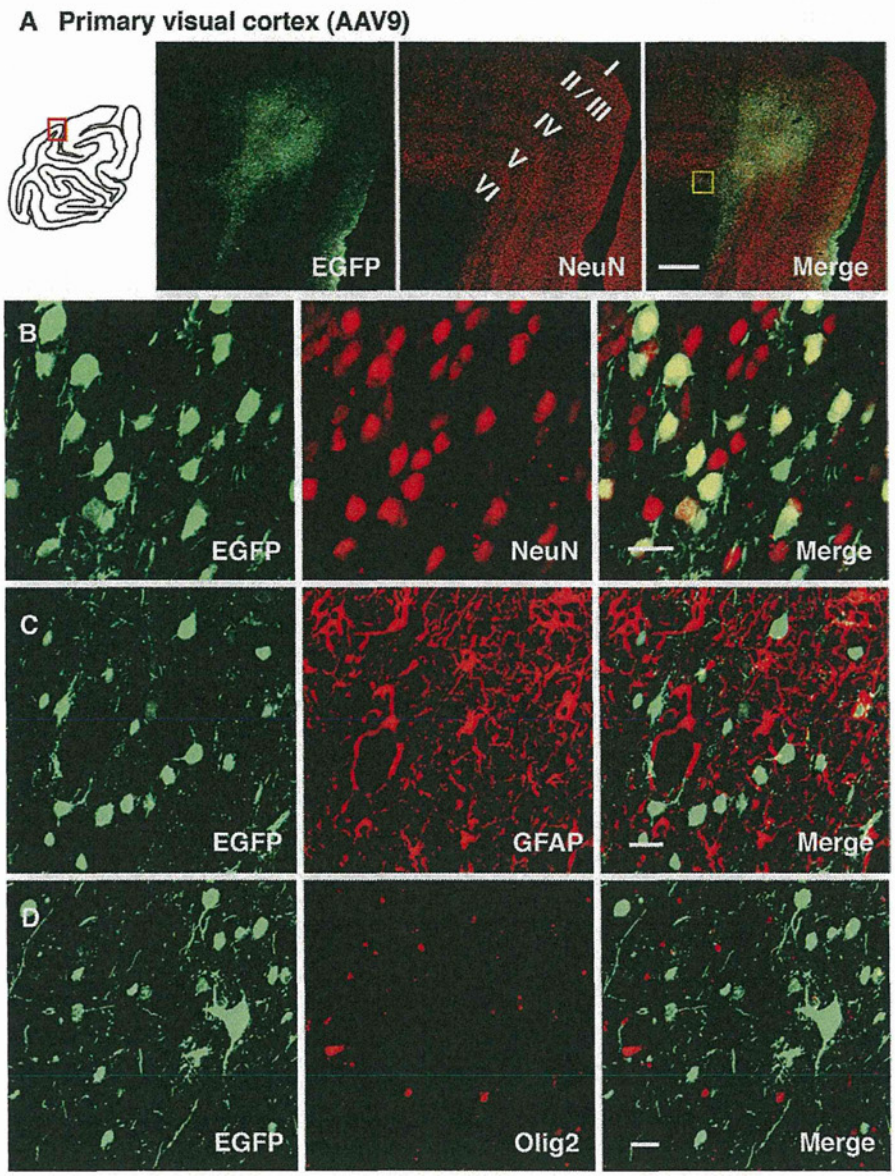

Fig. 2. Gene transfer into neurons of the primary visual cortex of macaque monkeys with AAV9. (A) Low power confocal images at the injection site, approximately corresponding to the red box on a coronal section of the macaque brain map (left). The confocal images reveal prominent EGFP fluorescence around the injection site (green) and NeuN signals (red). (B) Confocal images reveal co-expression of EGFP (green) and NeuN (red), as shown by the merged image (yellow). The view field approximately corresponds to the yellow box on the right panel of (A). (C, D) EGFP-positive cells rarely co-express GFAP (red) or Olig2 (red), as shown by the merged images. Bars=500 μm in (A) and 20 μm in (B–D). The abbreviations are as listed in Fig. 1.

without the use of ion-exchange chromatography. More importantly, results from Foust et al. demonstrated that AAV9 crossed the blood–brain barrier in mice and cynomolgus monkeys, which offers a method for brain-wide gene delivery with less invasiveness, especially for gene therapy applications.

The present study revealed, for the first time, neuronal infection patterns of AAV8 and AAV9 in the primate brain. AAV8, as well as AAV9, exhibited both local and retrograde infection patterns in nigrostriatal, corticostriatal, thalamostriatal and geniculocortical pathways. In the LGN, EGFP labeling was apparently restricted to the parvocellular layers. This observation, together with the observation of a lack of retrograde labeling in other brain regions, which are known to have connections with V1, may suggest that retrograde gene transfer after injection of AAV8 or AAV9 into the V1 are limited to the parvocellular layers of the LGN, although future experiments are required to obtain concrete evidence. For both AAV8 and AAV9, the number of neurons expressing EGFP by retrograde trans-

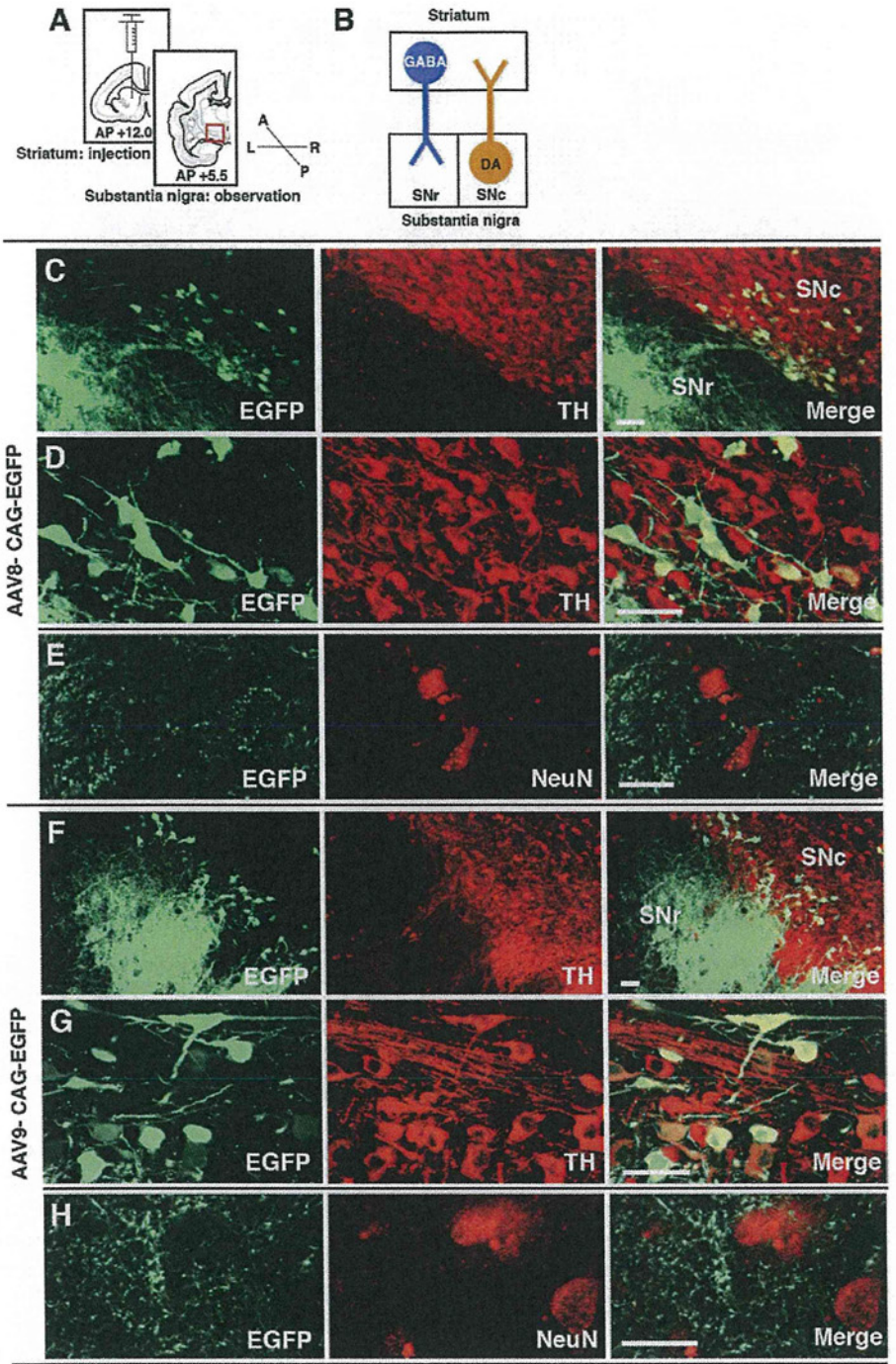

Fig. 3. Local and retrograde gene transfer into the marmoset nigrostriatal pathway with AAV8 and AAV9. (A) Experimental design. EGFP fluorescence is detected in the substantia nigra (red box) following AAV8-EGFP or AAV9-EGFP injection into the striatum. A, anterior; P, posterior; R, right; L, left. (B) Schematic diagram of the nigrostriatal pathway. GABAergic neurons in the striatum (GABA, blue) project to the SNr, and dopaminergic neurons (DA, orange) in the SNc project to the striatum. (C, F) EGFP fluorescence is observed in axon terminals in the SNr, as well as in cell bodies of the SNc following AAV8 (C) or AAV9 (F) injection. (D, G) High-power images of the SNc. EGFP-positive cell bodies (green) co-express TH (red), as shown by the merged images (yellow). (E, H) High-power images of the SNr. EGFP-positive fibers and varicosities (green) are evident around NeuN-positive cell bodies (red). Bars=50 μm in (C, D, F, G) and 20 μm in (E, H). AAV8, adeno-associated virus serotype 8; DA, dopamine; GABA, gamma-aminobutyric acid; SNc, substantia nigra pars compacta; SNr, substantia nigra pars reticulata; TH, tyrosine hydroxylase. Other abbreviations are as listed in Fig. 1.

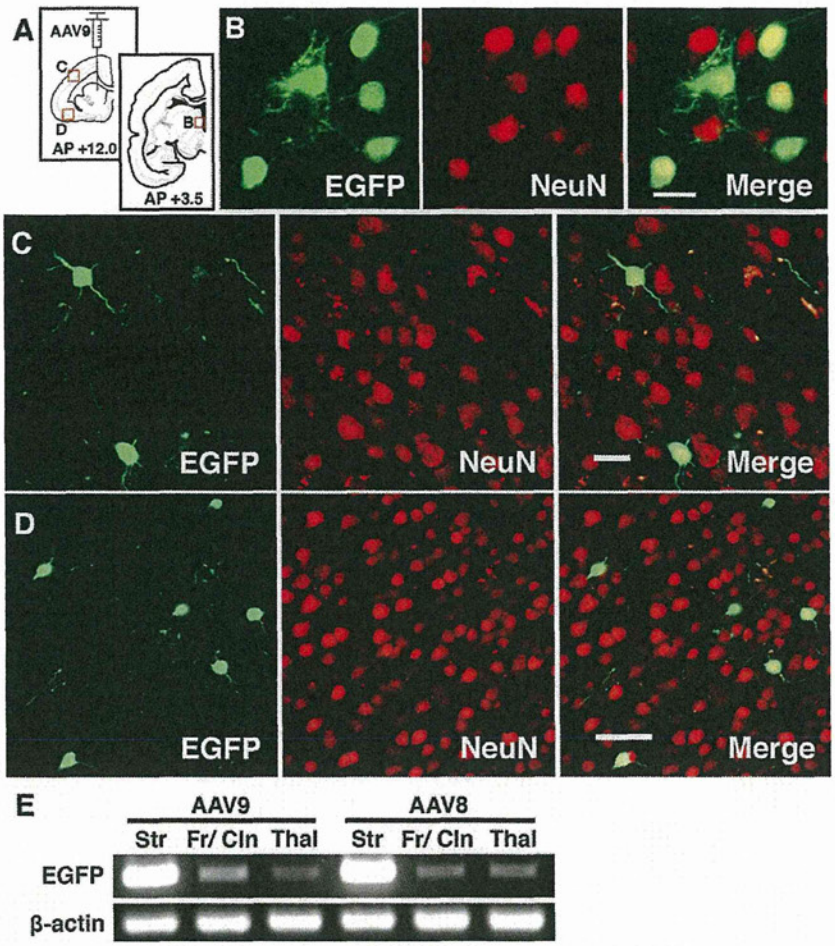

Fig. 4. Retrograde gene transfer into neurons of the frontal/insular cortices and thalamus following AAV9 injection into the striatum. (A) AAV9-EGFP was injected into the striatum at anteroposterior (AP) +12 mm. Retrograde EGFP labels were detected in the thalamus, probably corresponding to the parafascicular thalamic nucleus (B), the frontal cortex (C), and the insular cortex (D). (B–D) Confocal images indicate co-expression of EGFP (green) and NeuN (red) in the thalamus (B), the frontal cortex (C), and the insular cortex (D), as shown in the merged images (yellow). (E) Polymerase chain reaction (PCR) analyses reveal the presence of viral transgene (EGFP) not only in the striatal local infection site (Str), but also in the frontal/insular cortices (Fr/Cln) and the thalamus (Thal) in which cell bodies with retrograde EGFP fluorescence were observed. Bars=20 μm in (B, C) and 50 μm in (D). PCR, polymerase chain reaction. Other abbreviations are as listed in Fig. 1.

fer was modest in the substantia nigra and relatively small in the LGN. Transgene expression was examined at 4 weeks after viral injection; however, the time frame may be insufficient for acquiring full transgene expression in the somata via retrograde transport. In general, AAV-mediated transgene expression persists for long periods (more than a year), and long-term expression would allow for improved efficiency of neuronal transgene expression via retrograde AAV transport.

In the present study, we conducted PCR analyses and confirmed the presence of viral transgenes in the neuronal somata following retrograde infections of either AAV8 or AAV9. These results prove that the genome of AAV8 or AAV9 itself is transported to the soma after retrograde infection at the axon terminal in the brain. This probable mechanism has been demonstrated in several other AAV serotypes, such as AAV1, AAV2, and AAV6 (Kaspar et al., 2002; Hollis et al., 2008; Towne et al., 2010).

A number of neuroscience studies have demonstrated the roles of hierarchical and interconnected structures of the brain in terms of information processing for cognition and behavior (Felleman and Van Essen, 1991; Murphy and Sillito, 1996; Nishimura et al., 2007; Bostan et al., 2010). Retrograde neuronal delivery of molecular tools through the use of AAV8 or AAV9 vectors could provide methods for analyzing hierarchical information processing in the brain. For example, injection of recombinant AAV8 or AAV9 expressing transgenes encoding optogenetic tools into a given brain region could lead to transgene neuronal delivery with direct projections to the injected site, thereby allowing for experimental *in vivo* manipulation of neuronal inputs to the injected brain area. Therefore, transgene

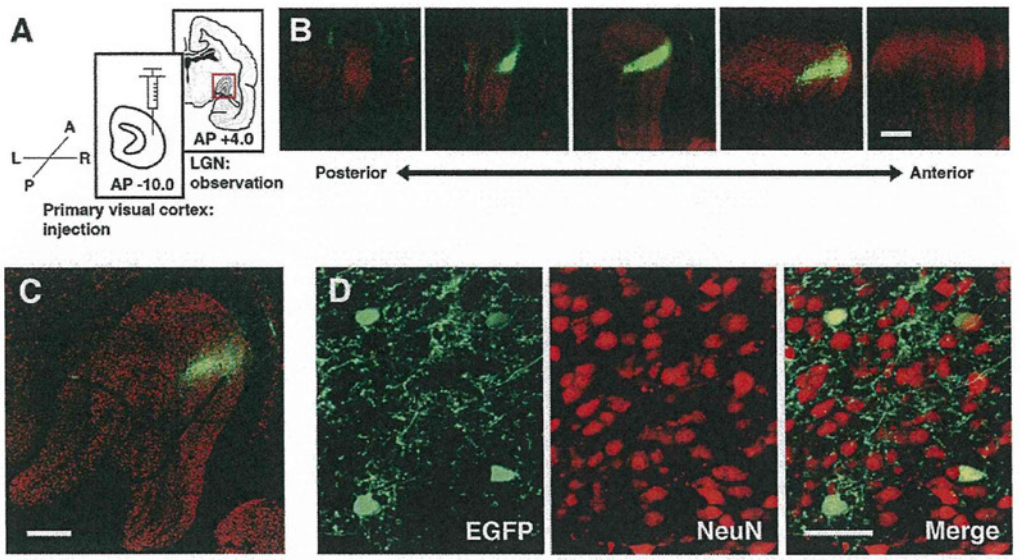

Fig. 5. Local and retrograde gene transfer into the marmoset geniculocortical pathway with AAV9. (A) Experimental design. EGFP expression is visible in the LGN (red box) following injection of AAV9-EGFP into the primary visual cortex. (B) Confocal images of EGFP fluorescence (green) and NeuN expression (red) in coronal sections of the LGN, approximately 3.4–4.2 mm anterior to the interaural line. (C) Representative coronal section of the LGN around the center of EGFP expression (green) overlaid on NeuN signals (red). Approximately 4.0 mm anterior to the interaural line. (D) High-power confocal images show EGFP-positive cell bodies, axons and varicosities (green) in the LGN. EGFP-positive cell bodies co-express NeuN (red), as shown by the merged image (yellow). Bars=500 μm in (B, C) and 50 μm in (D). LGN, lateral geniculate nucleus. Remaining abbreviations are as listed in Fig. 1.

delivery into primate brains via AAV8 and AAV9 vectors could facilitate studies focused on circuit-based principles of brain function by utilizing high-infection efficiencies, as well as neuronal infection patterns.

CONCLUSIONS

Results from the present study, in combination with our previous study, revealed that AAV8 and AAV9 exhibited strong endogenous tropism for neurons in primate brains. The present results further demonstrated that these AAV serotypes can infect neurons both locally and retrogradely. These infection patterns allow transgene delivery to local neurons surrounding virus-injection sites via local infection from somata/dendrites, as well as to distal neurons that project to virus-injection sites via retrograde infections from axon terminals.

Acknowledgments—We thank Dr. James M. Wilson for providing helper plasmids pAAV2-8 (originally described as p5E18-VD2/8) and pAAV2-9. This study was supported by the JSPS Research Fellowship for Young Scientists (Y.M.) and by PRESTO, JST (K.N.). All authors declare no conflict of interest.

REFERENCES

Albin RL, Young AB, Penney JB (1989) The functional anatomy of basal ganglia disorders. Trends Neurosci 12:366–375.

Alexander GE, Crutcher MD (1990) Functional architecture of basal ganglia circuits: neural substrates of parallel processing. Trends Neurosci 13:266–271.

Bostan AC, Dum RP, Strick PL (2010) The basal ganglia communicate with the cerebellum. Proc Natl Acad Sci U S A 107:8452–8456.

Broekman ML, Comer LA, Hyman BT, Sena-Esteves M (2006) Adeno-associated virus vectors serotyped with AAV8 capsid are more efficient than AAV-1 or -2 serotypes for widespread gene delivery to the neonatal mouse brain. Neuroscience 138: 501–510.

Chan AW, Chong KY, Martinovich C, Simerly C, Schatten G (2001) Transgenic monkeys produced by retroviral gene transfer into mature oocytes. Science 291:309–312.

Dodiya HB, Bjorklund T, Stansell J, III, Mandel RJ, Kirik D, Kordower JH (2010) Differential transduction following basal ganglia administration of distinct pseudotyped AAV capsid serotypes in nonhuman primates. Mol Ther 18:579–587.

Eslamboli A, Georgievska B, Ridley RM, Baker HF, Muzyczka N, Burger C, Mandel RJ, Annett L, Kirik D (2005) Continuous low-level glial cell line-derived neurotrophic factor delivery using recombinant adeno-associated viral vectors provides neuroprotection and induces behavioral recovery in a primate model of Parkinson's disease. J Neurosci 25:769–777.

Felleman DJ, Van Essen DC (1991) Distributed hierarchical processing in the primate cerebral cortex. Cereb Cortex 1:1–47.

Foust KD, Nurre E, Montgomery CL, Hernandez A, Chan CM, Kaspar BK (2009) Intravascular AAV9 preferentially targets neonatal neurons and adult astrocytes. Nat Biotechnol 27:59–65.

Foust KD, Wang X, McGovern VL, Braun L, Bevan AK, Haidet AM, Le TT, Morales PR, Rich MM Burghes AH, Kaspar BK (2010) Rescue of the spinal muscular atrophy phenotype in a mouse model by early postnatal delivery of SMN. Nat Biotechnol 28:271–274.

Fritsches KA, Rosa MG (1996) Visuotopic organisation of striate cortex in the marmoset monkey (Callithrix jacchus). J Comp Neurol 372:264–282.

Gao G, Vandenberghe LH, Alvira MR, Lu Y, Calcedo R, Zhou X, Wilson JM (2004) Clades of Adeno-associated viruses are widely disseminated in human tissues. J Virol 78:6381–6388.

Gao GP, Alvira MR, Wang L, Calcedo R, Johnston J, Wilson JM (2002) Novel adeno-associated viruses from rhesus monkeys

as vectors for human gene therapy. Proc Natl Acad Sci U S A 99:11854–11859.

Han X, Qian X, Bernstein JG, Zhou HH, Franzesi GT, Stern P, Bronson RT, Graybiel AM, Desimone R, Boyden ES (2009) Millisecond-timescale optical control of neural dynamics in the nonhuman primate brain. Neuron 62:191–198.

Hollis ER, II, Kadoya K, Hirsch M, Samulski RJ, Tuszynski MH (2008) Efficient retrograde neuronal transduction utilizing self-complementary AAV1. Mol Ther 16:296–301.

Kaplitt MG, Leone P, Samulski RJ, Xiao X, Pfaff DW, O'Malley KL, During MJ (1994) Long-term gene expression and phenotypic correction using adeno-associated virus vectors in the mammalian brain. Nat Genet 8:148–154.

Kaspar BK, Erickson D, Schaffer D, Hinh L, Gage FH, Peterson DA (2002) Targeted retrograde gene delivery for neuronal protection. Mol Ther 5:50–56.

Masamizu Y, Okada T, Ishibashi H, Takeda S, Yuasa S, Nakahara K (2010) Efficient gene transfer into neurons in monkey brain by adeno-associated virus 8. Neuroreport 21:447–451.

Matsushita T, Elliger S, Elliger C, Podsakoff G, Villarreal L, Kurtzman GJ, Iwaki Y, Colosi P (1998) Adeno-associated virus vectors can be efficiently produced without helper virus. Gene Ther 5:938–945.

Minamimoto T, Hori Y, Kimura M (2009) Roles of the thalamic CM-PF complex-Basal ganglia circuit in externally driven rebias of action. Brain Res Bull 78:75–79.

Murphy PC, Sillito AM (1996) Functional morphology of the feedback pathway from area 17 of the cat visual cortex to the lateral geniculate nucleus. J Neurosci 16:1180–1192.

Nakahara K, Adachi Y, Osada T, Miyashita Y (2007) Exploring the neural basis of cognition: multi-modal links between human fMRI and macaque neurophysiology. Trends Cogn Sci 11:84–92.

Nakahira E, Yuasa S (2005) Neuronal generation, migration, and differentiation in the mouse hippocampal primoridium as revealed by enhanced green fluorescent protein gene transfer by means of in utero electroporation. J Comp Neurol 483:329–340.

Nishimura Y, Onoe H, Morichika Y, Perfiliev S, Tsukada H, Isa T (2007) Time-dependent central compensatory mechanisms of finger dexterity after spinal cord injury. Science 318:1150–1155.

Okada T, Nomoto T, Yoshioka T, Nonaka-Sarukawa M, Ito T, Ogura T, Iwata-Okada M, Uchibori R, Shimazaki K, Mizukami H, Kume A, Ozawa K (2005) Large-scale production of recombinant viruses by use of a large culture vessel with active gassing. Hum Gene Ther 16:1212–1218.

Okada T, Nonaka-Sarukawa M, Uchibori R, Kinoshita K, Hayashita-Kinoh H, Nitahara-Kasahara Y, Takeda S, Ozawa K (2009) Scalable purification of adeno-associated virus serotype 1 (AAV1) and AAV8 vectors, using dual ion-exchange adsorptive membranes. Hum Gene Ther 20:1013–1021.

Okada T, Shimazaki K, Nomoto T, Matsushita T, Mizukami H, Urabe M, Hanazono Y, Kume A, Tobita K, Ozawa K, Kawai N (2002) Adeno-associated viral vector-mediated gene therapy of ischemia-induced neuronal death. Methods Enzymol 346:378–393.

Passingham R (2009) How good is the macaque monkey model of the human brain? Curr Opin Neurobiol 19:6–11.

Sasaki E, Suemizu H, Shimada A, Hanazawa K, Oiwa R, Kamioka M, Tomioka I, Sotomaru Y, Hirakawa R, Eto T, Shiozawa S, Maeda T, Ito M, Ito R, Kito C, Yagihashi C, Kawai K, Miyoshi H, Tanioka Y, Tamaoki N, Habu S, Okano H, Nomura T (2009) Generation of transgenic non-human primates with germline transmission. Nature 459:523–527.

Tan EM, Yamaguchi Y, Horwitz GD, Gosgnach S, Lein ES, Goulding M, Albright TD, Callaway EM (2006) Selective and quickly reversible inactivation of mammalian neurons in vivo using the Drosophila allatostatin receptor. Neuron 51:157–170.

Taymans JM, Vandenberghe LH, Haute CV, Thiry I, Deroose CM, Mortelmans L, Wilson JM, Debyser Z, Baekelandt V (2007) Comparative analysis of adeno-associated viral vector serotypes 1, 2, 5, 7, and 8 in mouse brain. Hum Gene Ther 18:195–206.

Towne C, Schneider BL, Kieran D, Redmond DE, Jr, Aebischer P (2010) Efficient transduction of non-human primate motor neurons after intramuscular delivery of recombinant AAV serotype 6. Gene Ther 17:141–146.

White AJ, Wilder HD, Goodchild AK, Sefton AJ, Martin PR (1998) Segregation of receptive field properties in the lateral geniculate nucleus of a New-World monkey, the marmoset Callithrix jacchus. J Neurophysiol 80:2063–2076.

Yasuda T, Miyachi S, Kitagawa R, Wada K, Nihira T, Ren YR, Hirai Y, Ageyama N, Terao K, Shimada T, Takada M, Mizuno Y, Mochizuki H (2007) Neuronal specificity of alpha-synuclein toxicity and effect of Parkin co-expression in primates. Neuroscience 144:743–753.

Yuasa S, Nakamura K, Kohsaka S (2010) Stereotaxic atlas of the marmoset brain with immunohistochemical architecture and MRI Images. National Institute of Neuroscience, National Center of Neurology and Psychiatry, Tokyo, Japan.

Zhang F, Wang LP, Brauner M, Liewald JF, Kay K, Watzke N, Wood PG, Bamberg E, Nagel G, Gottschalk A, Deisseroth K (2007) Multimodal fast optical interrogation of neural circuitry. Nature 446:633–639.

(Accepted 28 June 2011)
(Available online 18 July 2011)

NeuroImage 54 (2011) 203–212

Contents lists available at ScienceDirect

NeuroImage

journal homepage: www.elsevier.com/locate/ynimg

Technical Note

Simultaneous recording of ECoG and intracortical neuronal activity using a flexible multichannel electrode-mesh in visual cortex

Haruo Toda [a,*], Takafumi Suzuki [b], Hirohito Sawahata [a], Kei Majima [c,d], Yukiyasu Kamitani [c,d], Isao Hasegawa [a,*]

[a] Department of Physiology, Niigata University School of Medicine, Niigata, Japan
[b] Graduate School of Information Science and Technology, The University of Tokyo, Tokyo, Japan
[c] Department of Neuroinformatics, ATR Computational Neuroscience Laboratories, Kyoto, Japan
[d] Graduate School of Information Science, Nara Institute of Science and Technology, Nara, Japan

ARTICLE INFO

Article history:
Received 29 June 2010
Revised 28 July 2010
Accepted 3 August 2010
Available online 7 August 2010

ABSTRACT

Electrocorticogram (ECoG) is a well-balanced methodology for stably mapping brain surface local field potentials (LFPs) over a wide cortical region with high signal fidelity and minimal invasiveness to the brain tissue. To directly compare surface ECoG signals with intracortical neuronal activity immediately underneath, we fabricated a flexible multichannel electrode array with mesh-form structure using micro-electro-mechanical systems. A Parylene-C-based "electrode-mesh" for rats contained a 6×6 gold electrode array with 1-mm interval. Specifically, the probe had 800×800 μm^2 fenestrae in interelectrode spaces, through which simultaneous penetration of microelectrode was capable. This electrode-mesh was placed acutely or chronically on the dural/pial surface of the visual cortex of Long–Evans rats for up to 2 weeks. We obtained reliable trial-wise profiles of visually evoked ECoG signals through individual eye stimulation. Visually evoked ECoG signals from the electrode-mesh exhibited as well or larger signal amplitudes as intracortical LFPs and less across-trial variability than conventional silver-ball ECoG. Ocular selectivity of ECoG responses was correlated with that of intracortical spike/LFP activities. Moreover, single-trial ECoG signals carried sufficient information for predicting the stimulated eye with a correct performance approaching 90%, and the decoding was significantly generalized across sessions over 6 hours. Electrode impedance or signal quality did not obviously deteriorate for 2 weeks following implantation. These findings open up a methodology to directly explore ECoG signals with reference to intracortical neuronal sources and would provide a key to developing minimally invasive next-generation brain–machine interfaces.

Introduction

The local field potential (LFP) is a particular class of electrophysiological signals related to a summation of neural activity that has recently become of converging interest (Fries, 2009). Whereas the action potential or spike activity represents output signals from neurons typically located within 100 micrometers of an electrode tip, LFP is considered to arise primarily from excitatory and inhibitory dendritic potentials and afterdepolarization/hyperpolarization (Mitzdorf, 1985) and thus serve as a marker of inputs to and local processing within a volume of brain tissue extending at least several hundred micrometers (Katzner et al., 2009). LFP is also closely correlated with BOLD fMRI signals (Logothetis et al., 2001). Since various frequency components of LFPs have been implicated in carrying across cortical areas relevant sensory, motor or cognitive information (Buschman and Miller, 2007; Whittingstall and Logothetis, 2009), the need for recording LFPs from the global cortical circuits is increasing.

Electrocorticogram (ECoG) is one of the methodologies that enables global mapping of LFPs both in humans and animal models. Compared with microelectrode methods, ECoG has the advantage to record cortical surface LFPs less invasively across broader regions. Compared with scalp electroencephalogram, ECoG has better spatial resolution and signal fidelity (Chao et al., 2010; Gaillard et al., 2009; Leuthardt et al., 2006; Slutzky et al., 2010). In particular, high-density ECoG electrode array is a promising tool for electrophysiological mapping with millimeter precisions for source localization (Hollenberg et al., 2006; Rubehn et al., 2009; Yeager et al., 2008). However, it has been technically demanding to directly compare between surface ECoG and intracortical activity just underneath, because (1) penetrating the ECoG sheet is virtually impossible without damaging the microelectrode tip, and (2) the recording surface of ECoG electrode is too large (typically more than 2 mm in diameter) to allow simultaneous depth-recording within submillimeter.

* Corresponding authors. Fax: +81 25 227 0755.
E-mail addresses: toda@med.niigata-u.ac.jp (H. Toda), ihasegawa-nsu@umin.ac.jp (I. Hasegawa).

1053-8119/$ – see front matter © 2010 Elsevier Inc. All rights reserved.
doi:10.1016/j.neuroimage.2010.08.003

To address this issue, we developed a novel flexible ECoG probe (electrode-mesh) using micro-electro-mechanical systems (MEMS) technology (Takeuchi et al., 2005). The probe was designed to have a mesh structure for stable electrode contact to the curved brain surface, and for simultaneous penetration of microelectrodes through the fenestrae, or mesh holes. To test the feasibility of our method for combined ECoG and intracortical recordings, we applied the probe *in vivo* to the primary visual cortex (V1) of Long–Evans rats in acute as well as chronic preparation. We tested if multichannel ECoG signals could be reliably recorded in response to visual stimulation and examined correlation between epidural ECoG and intracortical spikes in terms of the ocular dominance index. We also evaluated the potential advantage of our method over conventional approaches by directly comparing the amplitude of visually evoked potentials or trial-to-trial signal variability among different probes.

Flexible ECoG probe is not only a promising electrophysiological tool for characterizing ensemble neural activity to code particular sensory stimuli or motor plans, but also an important candidate for the input device of brain–machine interfaces (BMIs) that predict stimuli or behaviors from neural responses (Kamitani and Tong, 2005; Lebedev and Nicolelis, 2006). Since safety of ECoG has been clinically ensured (Leuthardt et al., 2006), the ability to decode sensory- or motor-associated information from trial-wise ECoG signals would be critical for development of efficient BMI (Schwartz et al., 2006). Therefore, we tested whether single-trial ECoG signals contained sufficient information for predicting the stimulated eye by decoding analysis (Kamitani and Tong, 2005).

Methods

Structure and fabrication of an electrode-mesh

An electrode-mesh (Fig. 1a) was designed to contain 32-channel recording electrodes plus 2 reference/2 ground electrodes located at the crossings of the gold beams, or wirings (20-μm width). The interelectrode distance was 1 mm. At each electrode, gold surface was exposed in a square shape (50×50 μm). Since 5×5 square holes (800×800 μm per each) were open in the space between electrodes, the probe had a mesh structure. The whole mesh size was 6×6 mm, and a cable lead to a pad for a 0.025-inch pitch 36-pin connector (#A8828-001, Omnetics, MN, USA).

Fig. 1b shows the simplified fabrication process of the electrode-mesh. Detailed fabrication procedures for Parylen-C (poly(chloro-para-xylylene))-based electrodes were described elsewhere (Takeuchi et al., 2005). (1) At first, Parylene-C was deposited on a silicon substrate using a coating machine (PDS 2010, Specialty Coating Systems). Then a gold layer was deposited with a vacuum evaporator (SVC-700, Sanyu, Japan) and patterned by wet etching. (2) Parylene-C was deposited again, and aluminum was also deposited and patterned by wet etching. (3) Parylene-C layer was patterned by an oxygen plasma etching system (FA-1, Samco, Japan). The aluminum layer worked as a mask and was removed after the process. (4) Finally, the probes were peeled off the silicon substrate by tweezers, and all recording electrodes were coated with platinum black by electrochemical plating. An example of the final product is shown in Figs. 1c and d.

Animal preparation for ECoG/LFP/spike recordings

A schematic illustration of the recording setup is shown in Fig. 1e. In acute main experiments, data were obtained from six hemispheres in three adult rats (Long–Evans, 300–400 g). The rats were anesthetized by intraperitoneal injection of urethane (0.5 ml of 30% solution/100 g body weight). The anesthetized rats were restrained to the stereotaxic apparatus (SR-5, Narishige, Tokyo, Japan) with their head fixed. Part of the cranium was removed to place the electrode-mesh on the dura mater and to allow tungsten microelectrode penetrations into the cortex (Fig. 1f). To suppress the pulsation and drying of the brain, we placed cotton filled with saline on the dura. The craniotomized areas were 2–9 mm posterior and 1–7 mm lateral to bregma. These areas corresponded to V1 and the adjacent secondary visual cortex (V2) except for the posterior tip of V1 (Fig. 2a) in the unrolled cortical map reconstructed from the rat brain (Paxinos and Watson, 2007). The anterior end of the electrode-mesh was located on the parietal association cortices. The positional errors of the electrode-mesh with reference to the 5 stereotaxic coordinates were <1 mm in each direction. A combination of a Roman numeral (mediolateral coordinate) and an alphabetical character (anterioposterior coordinate) is used to refer to a particular channel in the electrode-mesh. A tungsten microelectrode with an impedance of 0.5 MΩ or 1 MΩ (World Precision Instruments, FL, USA) was penetrated via the electrode-mesh into the cortex to record neuronal spikes and intracortical LFP (icLFPs) in combination with epidural activities. We additionally conducted control experiments in four hemisphere of two adult rats (Long–Evans, 300–400 g). In the control experiments, conventional silver-ball ECoG electrode with a 1-mm diameter (EKL-02010-03, Bioresearch Center, Tokyo, Japan) was softly attached to the dura mater by a manipulator fixed to the stereotaxic apparatus through a fenestra of the electrode-mesh. We carefully monitored the animals' eyes and were ready to place a drop of sodium hyaluronate to prevent the eyes from being dried out. In most cases, the eyes were naturally wet for hours, and no animals did develop cataract at the end of the experiment. A typical combined recording session took 3–6 hours in both main and control experiments.

Other six adult rats (Long–Evans, 200–300 g) were used in chronic implantation experiments. The rat was anesthetized by intraperitoneal injection of sodium pentobarbitulate (Nembutal, 0.1 ml/100 g body weight). Two stainless steel screws for anchor and electrode reference were implanted at 2 mm rostral of the bregma. Craniotomy was performed in the same way as described above and an electrode-mesh was placed on the V1 epidurally ($n=2$) or subdurally ($n=4$). The electrode-mesh was covered with a gelatine sponge (Gelfoam, Pfizer) and fixed on the skull with a dental resin. After implantation, the impedance of the electrodes was measured under Nembutal anesthesia in every 3 or 4 days with an IMP-2 impedance meter (BAK electronics, MD, USA). In four rats, visually evoked responses were recorded in the 14th day of implantation in the same way as acute experiments.

All the experimental procedures were approved by the Niigata University Animal Experiment Committee and conformed to guidelines of the animal welfare laws in Japan and NIH Guide for the Care and Use of Laboratory Animals.

Visual stimulation

The anesthetized animal was placed 28.6 cm in front of a 19-inch (90 degree in visual angle) cathode ray tube display monitor (EIZO T561, Nanao, Ishikawa, Japan). Visual stimuli were presented to the full field of the display except for part of the lower visual field occluded by the incisor bar of the stereotactic apparatus. The effective horizontal and vertical visual angles for the animal were 80 degree and 40 degree, respectively. Visual stimuli were moving sinusoidal gratings generated using ViSaGe (Cambridge Research Systems, UK) controlled by a software written in FreePascal/Lazarus and run on Windows XP. Spatial (0.04–0.15 cycle/deg) and temporal (3–7 Hz) frequencies of the gratings were optimized according to Girman et al. (1999). Stimulus duration was 500 ms and the inter-trial interval was pseudo-randomized between 1.5 and 2.0 sec. In the contralateral-eye stimulation (Contra) or ipsilateral-eye stimulation (Ipsi) conditions, the eye ipsilateral or contralateral to the recorded hemisphere, respectively, was covered with an eye patch. Stimulation was performed in separate blocks consisting of 40–200 trials. In certain

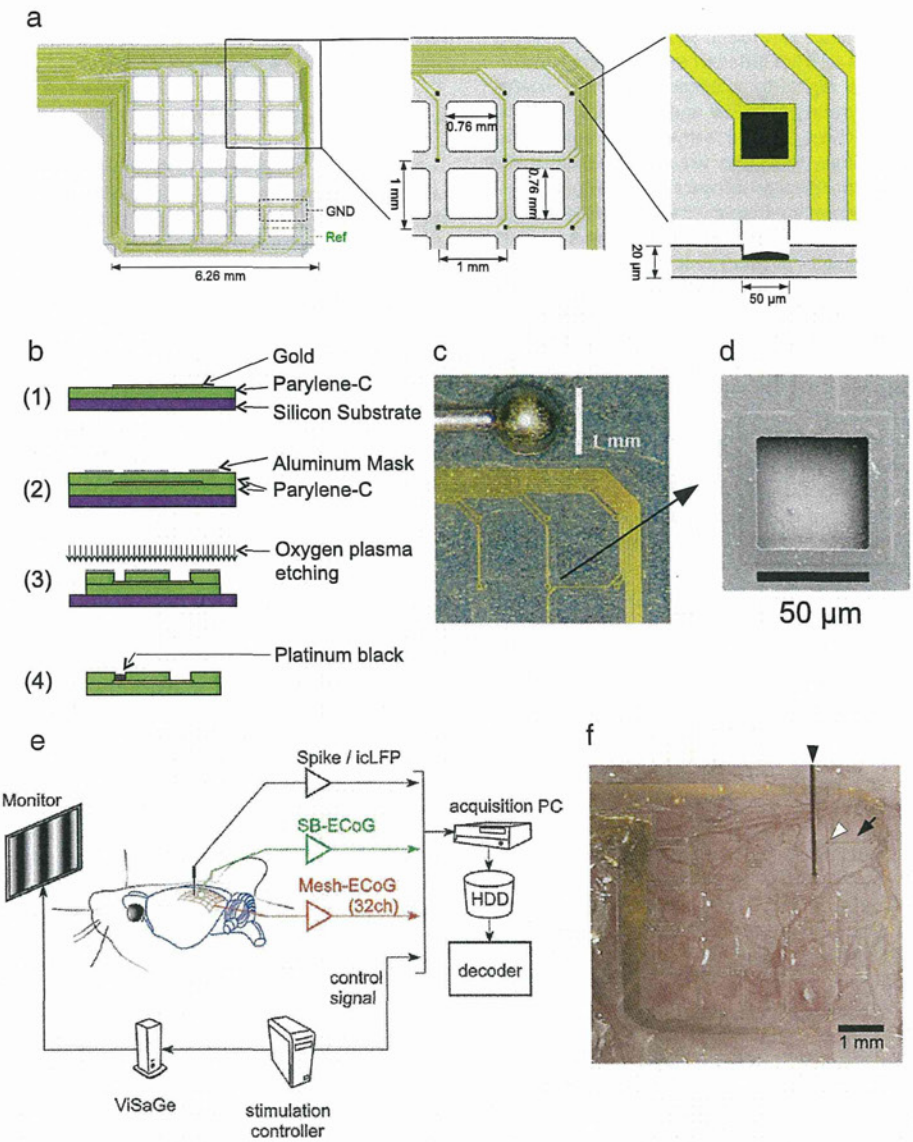

Fig. 1. Flexible electrode-mesh: structure, fabrication and in vivo application. (a) Structure of an electrode-mesh. Thirty-six gold electrodes (50×50 μm) were arranged in a 6×6 array with 1-mm interelectrode intervals, wired within a flexible Parylene-C (poly(chloro-para-xylylene)) substrate of 20 μm thick, and connected to a terminal. Between electrodes, holes (800×800 μm) were open through the substrate. Black and green dotted boxes: electrodes for signal ground and reference, respectively. (b) Simplified fabrication process of the electrode-mesh: (1) Following deposition of Parylene-C on a silicon substrate, a gold layer was deposited and patterned by wet etching. (2) Parylene-C was deposited again, and an aluminum mask layer was deposited and patterned by wet etching. (3) Parylene-C was patterned by an oxygen plasma etching and the aluminum mask was removed. (4) The probe was peeled off the silicon substrate, and coated with platinum black. (c) A part of electrode-mesh, comparing to a conventional silver-ball ECoG electrode with a 1-mm diameter. (d) A scanning electron microscopy of a single electrode of an electrode-mesh. (e) Experimental setup for *in vivo* application of the electrode-mesh. During visual stimulation, multichannel ECoGs via an electrode-mesh (mesh ECoG), single-channel ECoG via a silver-ball ECoG electrode (SB) and spikes or intracortical LFPs (icLFP) via a tungsten microelectrode were simultaneously recorded from rat visual cortex. (f) Epidural placement of an electrode-mesh and a tungsten microelectrode. White arrowhead: one of the ECoG electrodes. Black arrowhead: a tungsten microelectrode penetrated through one of the holes. Arrow: gold beam for wiring.

trials, both eyes were covered with eye patches to ensure that the visual stimuli were effectively blocked. In additional experiments, we used a video oculography (ET-60-L, Newopto Co. Ltd., Kawasaki, Japan) to ensure that no voluntary eye movements or microsaccades occurred during visual stimulation under anesthesia.

Data acquisition and processing

Multichannel ECoG signals were differentially amplified using a 32-channel Plexon amplifier (Plexon, TX, USA) with 300 Hz and 0.7 Hz high- and low-cutoff filters, respectively. The signal references for multichannel ECoGs were connected to the reference on the electrode-mesh. In the main experiments, signals from the tungsten microelectrode were amplified using a DAM-80 AC amplifier (World Precision Instruments, FL, USA) with a wide-band filter (10 kHz and 1 Hz high- and low-cut frequencies, respectively). In control experiments, signals from the silver-ball electrode and the tungsten microelectrode were amplified by 8-channel Plexon amplifier with a wide-band filter (8 kHz and 0.7 Hz high- and low-cutoff frequencies). For microelectrode or silver-ball electrode recordings, signal references were connected to the animal at the neck muscle unless otherwise stated. In chronic implantation experiments, the reference